

FlexiSCD: Flexible Surface Code Deformer for Dynamic Defects

Keyi Yin¹, Xiang Fang², Travis Humble³, Ang Li⁴, Yunong Shi⁵, and Yufei Ding¹

¹University of California, San Diego, CA, USA

²University of California, Santa Barbara, CA, USA

³Oak Ridge National Laboratory, Oak Ridge, TN, USA

⁴Pacific Northwest National Laboratory, Richland, WA, USA

⁵AWS Quantum Technologies, New York, NY, USA

Abstract—Quantum Error Correction (QEC) codes are vital for protecting quantum computers from noise by encoding quantum information redundantly in physical qubits. However, dynamic defects pose a significant challenge, potentially rendering physical qubits faulty during computation across various quantum platforms. Current defect mitigation strategies focus on surface codes, but often fail to fully restore QEC capability or disrupt logical operations.

In our paper, we introduce FlexiSCD, a code deformation framework that integrates adaptive defect mitigation into surface code workflows. It strategically crafts basic deformation instructions based on gauge transformations, enabling optimized processes tailored to specific defects, restoring QEC capability efficiently with fewer qubit resources. We also design an adaptive code layout for efficient logical operations.

Our evaluation demonstrates that FlexiSCD reduces failure rates by $35\times \sim 70\times$ and requires only half the qubit resources compared to previous methods. It surpasses previous defect removal techniques, preserving QEC capability and improving surface code communication.

I. INTRODUCTION

Device errors significantly hinder the advancement of quantum computing [3], obstructing its capability to fulfill its vast potential [4], [5], [6]. Consequently, Quantum Error Correction (QEC), a technique that protects quantum information by using redundant qubits, is pivotal to achieve scalable fault-tolerant quantum computing (FTQC) [7].

Among current QEC code proposals [8], [9], [10], [11], [12], [13], [14], *surface code* [10], [14], [15], [16] is a leading candidate to achieve FTQC due to its simple 2D-lattice topology and high tolerance to physical qubit errors. Due to their practicality, small-scale surface codes have been successfully demonstrated on several quantum computing platforms [17], [18], [19], [20].

However, scaling surface codes still presents several challenges, especially *dynamic defects* that emerge on quantum hardware during computation. Events like cosmic-ray strikes on superconducting devices can induce multi-bit burst errors (MBBEs) during computation, leading to defects with localized error rate spikes as high as 50% in affected regions [21], [22], [23], [24]. *Leakage errors* in all platforms remove the qubit states from the computation space, rendering them inoperable

and triggering high-weight correlated errors [25], [26]. Various factors [27], [28], [29] can cause *error drift* that increases the qubit error rate on different quantum platforms.

These defects can persist for thousands of QEC rounds before their effects go away [22], severely compromising the error correction capability of surface codes. Without mitigation, the logical error rate could potentially increase by a factor of 100 on average [2], [17]. Hence, it is imperative to develop appropriate mitigation strategies for dynamic defects to maintain surface codes' error correction ability.

Dynamic defects are an inherent aspect of quantum device physics, rendering them insurmountable through hardware mitigation alone [24], [30]. Thus, mitigation at the software level is crucial. Current hardware detectors [31], [32] can swiftly and accurately detect these defects using statistical methods. Using these defect data, software-level solutions can be developed to effectively manage dynamic defects. Currently, the two main software approaches for defect mitigation are *defect removal* and *code enlargement*, although each method comes with its own challenges.

A. Defect Removal excludes defective qubits from syndrome measurements during QEC cycles to ensure the accuracy of decoding and subsequent correction. One leading defect removal technique is *ASC* (Adaptive Surface Code) [1], which performs a simple transformation (known as *super-stabilizer* [33], [34], [35], [36], [37], [38]) for defect removal. Defect removal methods such as ASC face two issues:

(1) *Lack of Distance Recovery*: Defect removal methods remove defective qubits without introducing new ones, leading to a permanent reduction in code distance (Section II-A) and increasing program failure rate. Preemptively selecting a larger code size could mitigate this issue to some extent, but accurately allocating the right qubit resources for all defect patterns is a challenge, often resulting in either insufficient resource allocation or wastage of qubits.

(2) *Inability to Address Different Defect Types*: Defects in surface codes appear as either defective syndrome or data qubits and they can be further categorized by their spatial location as boundary, corner, and interior qubits. Current methods apply a uniform transformation to all defects, hindering them from

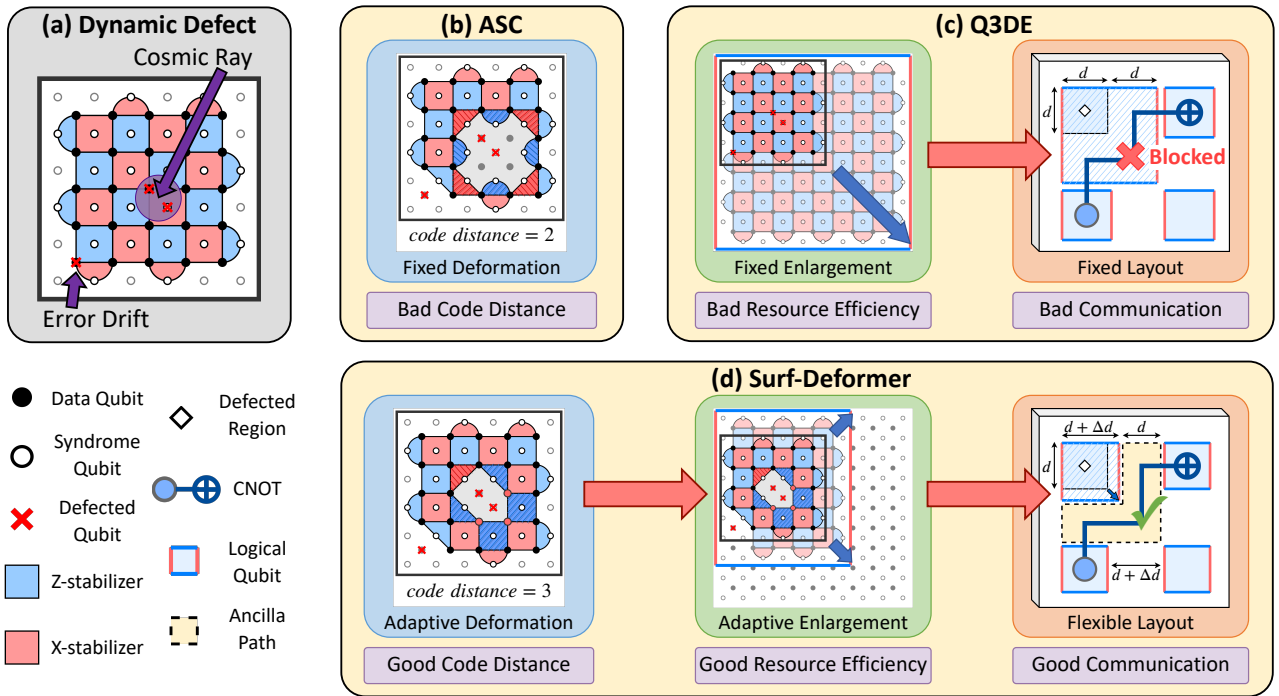


Fig. 1. Comparison of FlexiSCD with existing dynamic defect mitigation methods. (a) Illustration of dynamic defects induced by cosmic rays or error drift. (b) Adaptive Surface Code (ASC) [1] employs fixed deformation operation that leads to bad code distance. (c) Q3DE [2] utilizes fixed-scale enlargement on a fixed layout, resulting in poor resource utilization and communication efficiency. (d) FlexiSCD enables adaptive defect removal, enlargement, and layout optimization, providing a more versatile and efficient response to dynamic defects.

addressing specific defect types, which leads to suboptimal error correction capability in the resulting code.

B. Code enlargement preserves the code distance under defects by scaling up the code size. As an example, Q3DE [2], a leading enlargement method, initially spaces surface code patches by the code distance d (Fig. 1(c)). It then enlarges the code to a fixed size of $2d$ after defect detection (Fig. 1(c)), borrowing the “growth” transformation designed for *lattice-surgery* based logical operations [39]. Despite its simplicity, the Q3DE approach suffers from several drawbacks:

(1) *Increased Logical Error Rate*: Q3DE’s fixed-size enlargement cannot accommodate defect removal, allowing defects to persist and their errors to spread through surface code syndrome measurements, which leads to a significant increase in logical error rates (as detailed in Section II-A).

(2) *Qubit Resource Inefficiency*: Due to the lack of guarantee of the logical error rate, Q3DE pessimistically doubles code size after defects are detected, irrespective of their specific patterns. This often results in excessive enlargement beyond what’s needed for code distance restoration, leading to poor qubit resource efficiency.

(3) *Communication Impediment*: Q3DE focuses on recovering single code patches but overlooks the fact that doubled-size codes occupy the space between surface codes. This space is crucial for logical qubit communication in logical operations. This limitation results in significantly limited end-to-end system efficiency.

At a high level, the challenges faced by current defect

removal and enlargement approaches arise from their simple application of existing deformation methods, such as super-stabilizer and fixed-size enlarging. This rigid application limits their capacity to handle various defect types, enlarge incrementally, and integrate with each other effectively, resulting in high logical error rates.

Prompted by these challenges, we introduce FlexiSCD, a code deformation framework that extends the current surface code instruction set [40], [41], [42], [43] (detailed in Section II-C) to include adaptive defect mitigation capabilities. FlexiSCD meticulously crafts four deformation instructions (Section IV) that provides superior granularity and versatility compared to fixed operations in ASC and Q3DE.

FlexiSCD consists of two components: a compile-time *layout generator* and a runtime *code deformation unit*. The code deformation unit uses the extended instruction set to implement a highly optimized deformation strategy that unifies the defect removal and the enlargement approaches. This unified approach eliminates error sources from defects while restoring code distance, overcoming the limitations of ASC and Q3DE (Issue A.(1), B.(1)). Furthermore, due to FlexiSCD’s instruction design, the code deformation unit can effectively manage various defect types and facilitate adaptive enlargement, substantially improving error correction capabilities and resource efficiency (Issue A.(2), B.(2)). Additionally, the layout generator strategically adjusts the spacings between logical qubit patches to ensure unimpeded execution of two-qubit logical operations, thereby maintaining high end-to-end system efficiency (Issue

B.(3)). As a result, FlexiSCD resolves all issues of previous methods.

We perform a comprehensive evaluation of FlexiSCD. The end-to-end performance on various quantum programs shows that FlexiSCD considerably suppresses the program’s failure rate by $35\times \sim 70\times$ compared with ASC while maintaining nearly-optimal runtime, and requires only $\sim 50\%$ of Q3DE’s qubit resources. Ablation studies show that our framework significantly outperforms previous defect removal methods in preserving code distance and facilitates surface code communication by achieving nearly optimal throughput.

Our contributions can be summarized as follows:

- We introduce FlexiSCD, a deformation framework designed for adaptive defect mitigation on surface codes.
- We propose four meticulously crafted deformation instructions, offering highly flexible deformation strategies when combined.
- We establish a novel code deformation strategy based on our instructions, which not only unifies previous defect removal and enlargement methods but also yields more optimized deformation processes.
- We propose a novel surface code layout that achieves nearly optimal runtime while maintaining the target logical error rate, effectively resolving communication issues present in existing methods.

II. BACKGROUND AND MOTIVATION

A. Surface Codes

Surface codes arrange physical qubits on a 2D grid to collectively encode logical qubits. We illustrate its key components below as well as in Fig. 2.

Pauli operators. Pauli X and Z operators are fundamental qubit operations in QEC for describing both errors and error detection operations [44]. Importantly, X and Z anti-commute, *i.e.*, $XZ = -ZX$, allowing QEC codes to detect X - or Z -errors using the Pauli Z or X operator. Additionally, X or Z errors can be corrected by applying the X or Z operator because $X^2 = Z^2 = I$.

Data and Syndrome qubits. Physical qubits in surface codes are either data qubits or syndrome qubits. Data qubits (black dots) store the logical quantum state, while syndrome qubits (white dots) are for error detection of adjacent data qubits through stabilizer measurements.

Stabilizers. Each syndrome qubit is associated with a *stabilizer* [45], [46], composed of Pauli operators on adjacent data qubits which identifies the type of error and the specific data qubits for which the syndrome qubit is accountable. Interior and boundary surface code stabilizers measure four and two adjacent data qubits, respectively, depicted as squares for interiors and half-circles for boundaries. Stabilizers are distinguished into X -type (red boxes), which detect Z errors and Z -type (blue boxes), which detect X errors. Stabilizers are designed to commute, ensuring consistent error detection.

Code distance is the minimal number of physical errors that induce a logical operation (error). The code distance of a surface code equals to the number of data qubits on its edge

(Fig. 2(a)). A surface code with more physical qubits gives a larger code distance and has better error resilience [15], [47].

Impact of Defects. Dynamic defects manifest on either data or syndrome qubits, located within the code or along its boundaries (edges or corners), resulting in intricate defect patterns (Fig. 2(b)). Defective syndrome qubits with high error rates fail to provide accurate error information, which renders the stabilizer inoperable and may compromise the code distance by half or more. Defective data qubits consistently generate excessive errors that may surpass the code’s QEC capability, elevating the logical error rate by orders of magnitude [2].

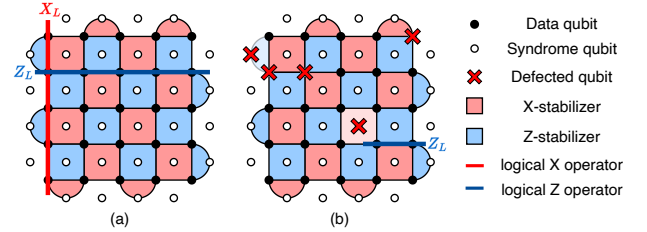


Fig. 2. (a) A surface code logical qubit with code distance 5. (b) A defective surface code logical qubit with code distance reduced to 2, illustrated by the weight-2 Z logical operator.

B. Gauge Transformation

Gauge transformation [48] is a fundamental technique that underpins FlexiSCD as well as facilitates logical operations on surface codes. In this section, we will introduce gauge operators and basic gauge transformations that can be viewed as atomic instructions on surface codes.

Gauge operators. Gauge refers to “degrees of freedom” in QEC. In surface codes, all Pauli operators that preserve logical qubit states are either stabilizers or logical operators, leaving no spare degrees of freedom. For purposes like defect mitigation, stabilizers can be converted to *gauge operators*, indicating that they are “set free”. This conversion can be simply done by ceasing the measurement of the selected stabilizers in QEC cycles. Gauge operators form anti-commutative pairs [49], meaning when a stabilizer is converted to a gauge operator, a corresponding Pauli operator that anti-commutes with it (but commutes with the rest of the stabilizers) is also introduced as a gauge operator (or more precisely, a generator of the gauge group [48]). One important utility of gauge operators is to provide freedom to measure stabilizers, *i.e.*, sometimes we can measure two gauge operators of which the product equals a stabilizer for syndrome measurement.

Gauge Transformation explores the degrees of freedom introduced by gauge operators. Converting stabilizers to gauge operators, as mentioned above, is an example of gauge transformations. There are four basic types of gauge transformation and they can be viewed as atomic instructions for performing operations on surface codes:

(1) *Stabilizer to Gauge (S2G):* S2G converts a stabilizer to a gauge operator. For example, in Fig. 3(c), the stabilizer s_1, s_2, g_1, g_2 are converted to gauge operators. Meanwhile,

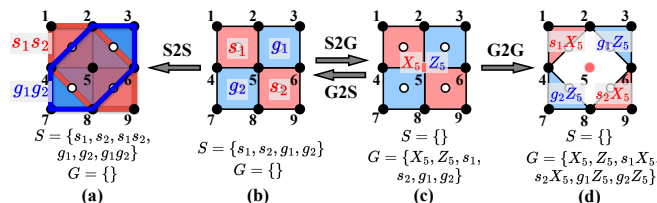


Fig. 3. Examples of basic gauge transformations.

X_5 and Z_5 , which anti-commute with g_1, g_2 and s_1, s_2 , are introduced. The updated stabilizer and gauge set become $S = \{\}$ and $G = \{X_5, Z_5, s_1, s_2, g_1, g_2\}$. This instruction potentially reduces the code size. S2G instructions are commutative, as they only depend on the set of newly introduced gauges.

(2) *Gauge to Stabilizer (G2S)*: G2S converts a gauge operator into a stabilizer and removes all gauge operators that anti-commute with it. G2S is the inverse process of S2G (Fig. 3(b)(c)). This instruction eliminates redundant degrees of freedom and expands the code.

(3) *Stabilizer to Stabilizer (S2S)*: S2S multiplies two stabilizers to form a new stabilizer. For instance, in Fig. 3(a), the product of stabilizers s_1, s_2 and g_1, g_2 , yields the stabilizers s_1s_2 and g_1g_2 . This instruction is often used to build larger stabilizers.

(4) *Gauge to Gauge (G2G)*: G2G multiplies two gauge operators to form a new gauge operator. For instance, in Fig. 3, the products of gauge operators s_1X_5, s_2X_5, g_1Z_5 , and g_2Z_5 also result in gauge operators. This instruction reorganizes gauge operators, potentially separating some qubit from the code. For example, the G2G transformation in Fig. 3(d) indicates that qubit q_5 can be separated from the code.

In summary, these four atomic instructions offer the building blocks for composing versatile and complex instructions to expand, contract, and deform the surface codes for purposes like performing logical operations and defect mitigation. Viewed as atomic instructions, they can be supported by any surface code implementation by simply altering the syndrome measurement patterns in QEC cycles.

C. Quantum Program Execution on Surface Codes

To execute a high-level quantum program on surface codes [40], [41], [42], [43], a compile time *algorithm compiler* first maps algorithmic qubits to surface code patches and lowers the logical operations to a native instruction schedule. During runtime, an *execution unit* utilizes this instruction schedule along with real-time data (such as syndrome measurement results) to execute the program.

Instruction set. Current implementations of surface code logical operations are predominantly based on the Lattice Surgery (LS) method [39], which provides an instruction set to expand and connect surface code patches to update and entangle logical states [48]. These instructions, such as *grow*, *merge*, and *split*, are composed of the atomic instructions introduced in Section II-B. For example, the *merge* instruction connects two arrays of physical qubit registers through a series of S2G and G2S transformations. In Fig. 4(b), applying *merge* to the

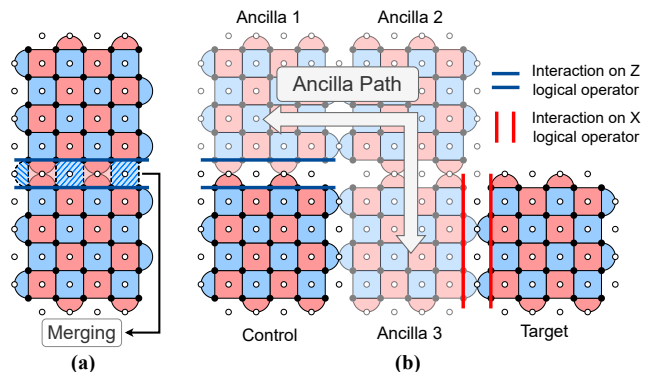


Fig. 4. (a) Example of merging two code patches. (2) Perform a logical CNOT gate on two distant logical qubits through an ancilla path connecting them. The control (resp. target) logical qubit interact with the ancilla logical qubit on the edge of Z- (resp. X-) logical operators, with equal-length interacting edges.

blue and red lines activates syndrome measurements on the ancillary patches between the logical surface code patches, facilitating a logical 2-qubit CNOT operation.

Code layout. Current surface code compilers as well as Q3DE arrange logical qubits on a grid with an inter-space of d , as shown in Fig. 4(b). This layout ensures that activated ancillary patches for logical operations maintain the same code distance as logical qubits, providing same level of noise protection.

III. THE FLEXISCD FRAMEWORK

The FlexiSCD framework consists of two main components: a compilation time *layout generator* and a runtime *code deformation unit*. As illustrated in Fig. 5, FlexiSCD integrates seamlessly with the existing surface code components, including the algorithm compiler and the execution unit.

The layout generator analyzes the input program to estimate the required number of logical qubits and the necessary code distance d to achieve a target logical error rate. It also computes the additional inter-space Δd based on the defect error model. This extra space accommodates potential enlargements and ensures communication between logical qubits during the execution of operations. We discuss the adaptive layout generator in detail in Section VI.

The code deformation unit is the core component of FlexiSCD. It deforms logical qubits dynamically to optimize defect mitigation during runtime. Utilizing real-time defect information from defect detectors and the current surface code configuration, the code deformation unit applies our adaptive deformation strategy. This strategy employs instructions from our extended instruction set to effectively remove defects and execute adaptive enlargements. The unit then forwards these instruction schedules to the execution unit for actual updates. Notably, despite the adaptiveness of our deformation methodology, actual code deformation updates can be implemented within a single QEC cycle.

We detail the extended instruction set in Section IV and the code deformation unit in Section V.

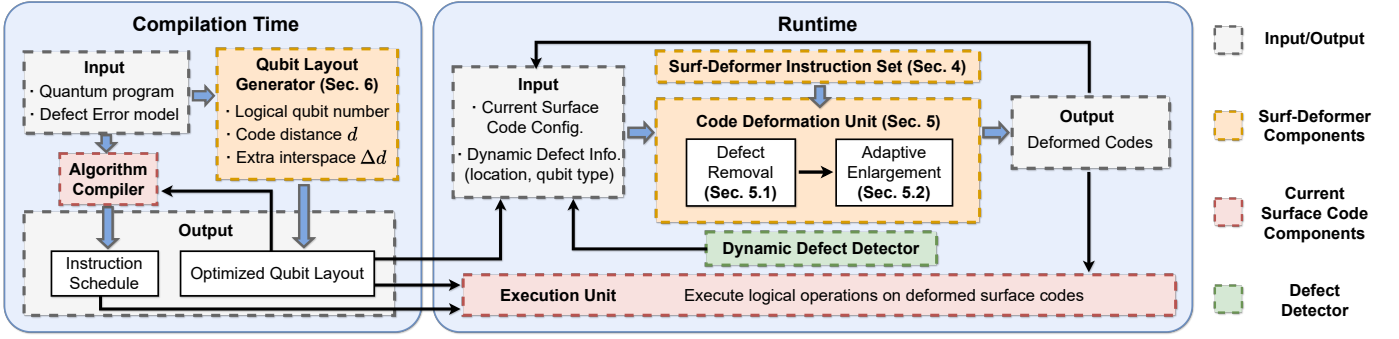


Fig. 5. FlexiSCD integrates a Qubit Layout Generator during compilation time and a Code Deformation Unit during runtime into the current surface code workflow. They are combined to extend adaptive defect mitigation functionality to the existing surface code implementation.

IV. THE FLEXISCD INSTRUCTION SET

Previous methods ASC and Q3DE are limited by their simplistic and fixed deformation operations for diverse defect patterns. In response, FlexiSCD introduces four carefully crafted instructions (Table I) to extend the current surface code instruction set (Section II-C). `DataQ_RM` and `SyndromeQ_RM` target the removal of interior data and syndrome qubits, respectively, while `PatchQ_RM` and `PatchQ_ADD` modify the boundaries of code patches to achieve adaptive boundary defect removal and code enlargement. Akin to CISC in classical computing, each instruction is constructed from multiple atomic instructions (Section II-B) adapted for the surface code topology, as detailed in Fig. 6. Meanwhile, these instructions are granular enough to ensure seamless integration and versatile enough to support a broad spectrum of deformation operations.

TABLE I
INSTRUCTION SETS OF VARIOUS SURFACE CODE IMPLEMENTATIONS

Method	Extended Instructions over LS	Supported Operations
Lattice Surgery	N/A	Logical operations
Q3DE	N/A	Logical operations, Fixed enlargement
ASC	<code>DataQ_RM</code>	Logical operations, Fixed qubit removal
FlexiSCD	<code>DataQ_RM</code> , <code>SyndromeQ_RM</code> , <code>PatchQ_RM</code> , <code>PatchQ_ADD</code>	Logical operations, Adaptive qubit removal, Adaptive enlargement

A. Code Deformation Instructions of FlexiSCD

Fig. 6 presents four deformation instructions introduced by FlexiSCD. Physical qubits are denoted by lattice coordinates, and boundaries by a list of qubit coordinates, both serving as input parameters of instructions.

(a) Data qubit removal (`DataQ_RM`): `DataQ_RM` removes a single data qubit. As shown in Fig. 6 (a), it first uses 4 $S2G$ to convert stabilizers s_1, s_2, g_1, g_2 into gauge operators, while introducing gauge operators Z_0, X_0 that anti-commute with s_1, s_2 and g_1, g_2 , respectively. It then uses 4 $G2G$ to adjust gauge

operators s_1, s_2, g_1, g_2 (rectangles) into $X_0s_1, X_0s_2, Z_0g_1, Z_0g_2$ (triangles), effectively separating q_0 from the code and enabling its removal. Notably, `DataQ_RM` coincides with ASC’s super-stabilizer method for single data qubit removal. However, within our framework, `DataQ_RM` is constructed explicitly and could be combined with other instructions to perform more versatile deformations, as will be shown in Section V.

(2) Syndrome qubit removal (`SyndromeQ_RM`): `SyndromeQ_RM` presents a novel method to remove a single syndrome qubit. It uses four $S2G$ to form $g_1 - g_4$. Interestingly, these four gauge operators form a new stabilizer (blue octagon in Fig. 6(b)) that doesn’t rely on q_0 . Meanwhile, four gauge operators $X_1 - X_4$ are introduced (red dots), and their product forms a stabilizer $X_{1,2,3,4}$. Measurement of $X_{1,2,3,4}$ can be achieved by using its constituent gauge operators without relying on the syndrome qubit q_0 , which allows the removal of q_0 from the code. This novel method maximizes the utility of adjacent intact data qubits and achieves optimal removal of a single interior syndrome qubit. Additionally, `SyndromeQ_RM` and `DataQ_RM` commute, as they both exclusively utilize $S2G$, which commute with themselves. This commutativity enables `SyndromeQ_RM` to be optimal even for complex defect patterns, as will be discussed in Section V.

(3) Boundary qubit removal (`PatchQ_RM`): `PatchQ_RM` removes defects on the boundary—for example, the syndrome qubit q_5 or data qubits q_1, q_2 in Fig. 6(c). This is achieved by combining several atomic instructions in Section II-B to deform the boundary, thus excluding the defects from the code patch. Fig. 6(c) presents an example where the boundary defective data qubit q_1 is removed by deforming the boundary from X_{L2} to X'_{L2} (specifically, we add and fix Z_1 as a stabilizer and update the rest of stabilizers and gauge operators accordingly).

(4) New qubits incorporation (`PatchQ_ADD`): The instruction `PatchQ_ADD` introduces new qubits beyond the original code. A new data qubit q is initialized in either the $|0\rangle$ or $|+\rangle$ state, equivalent to introducing a new stabilizer Z_q or X_q . New syndrome qubits are then added along with their associated stabilizers, which update the stabilizers and gauge operators through a series of atomic instructions (Section II-B), resulting in a deformed code containing additional qubits. Fig. 6(d) presents an example of adding two data qubits and

one syndrome qubit. This instruction can be iterated to facilitate code enlargement.

These four instructions can be combined to manage various defect types and facilitate adaptive code enlargement. The granularity and versatility provided by these instructions form the basis of our highly adaptive code deformation strategy, which will be detailed in Section V.

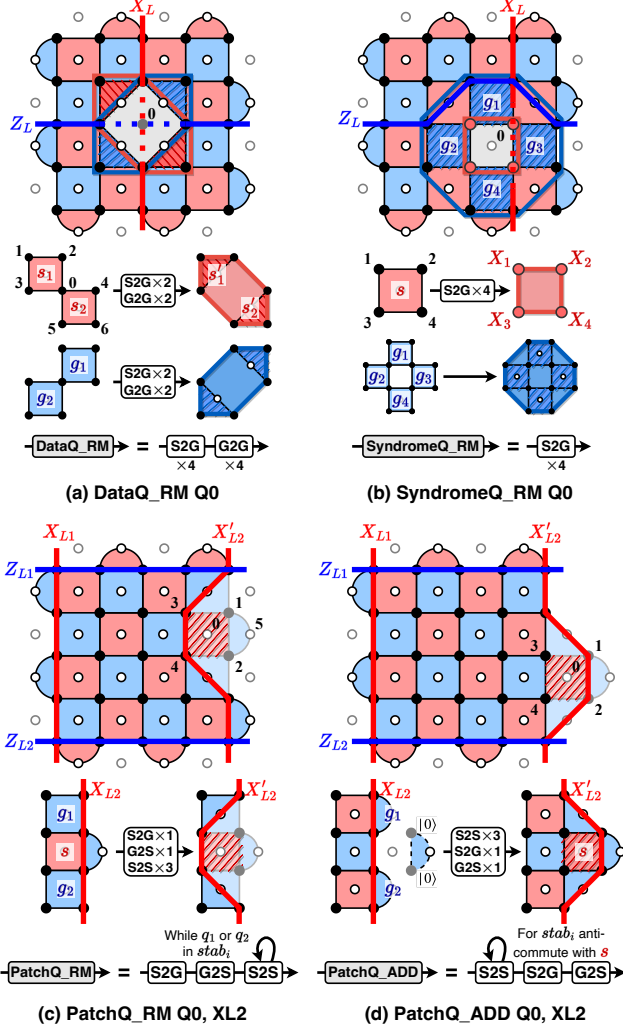


Fig. 6. Examples of the four deformation instructions of FlexiSCD. Q_i is the coordinate of qubit q_i and XL_j is the coordinate list that represents the boundary X_{Lj} .

V. THE CODE DEFORMATION UNIT

The code deformation unit is the core component of FlexiSCD for adaptive defect mitigation. Before every QEC cycle, the code deformation unit receives the current surface code configuration (including the shape and location of logical qubit patches) from the last round of deformation and current defect information from the dynamic defect detector. Leveraging this information, the code deformation unit executes two subroutines sequentially, as illustrated in Fig. 5. The first subroutine, *Defect Removal*, removes detected qubits from the current code. The second subroutine *Adaptive Enlargement* takes the resulting

code, calculates the new code distance, and adaptively enlarges the code.

A. Defect Removal Subroutine

The defect removal subroutine, outlined in Algorithm 1, is crafted to strategically handle various types of defects. Below, we detail the components of this algorithm:

Algorithm 1: Defect Removal Subroutine

Input: stabilizer set S , gauge set G ,
defective qubit set D
Output: stabilizer set S' , gauge set G'

```

1 for  $d_i \in D$  do
2   if  $d_i \in Interior\_Q$  then
3     if  $d_i \in Data\_Q$  then
4       DataQ_RM  $d_i$ 
5     else
6       SyndromeQ_RM  $d_i$ 
7     end
8   else
9     if  $d_i \in EdgeX\_Q$  and  $d_i \in EdgeZ\_Q$  then
10       $p_X, e_X = \text{find\_patch}(d_i, X)$ 
11       $p_Z, e_Z = \text{find\_patch}(d_i, Z)$ 
12       $p, e = \text{balancing}(p_X, e_X, p_Z, e_Z)$ 
13    else if  $d_i \in EdgeX\_Q$  then
14       $p, e = \text{find\_patch}(d_i, X)$ 
15    else
16       $p, e = \text{find\_patch}(d_i, Z)$ 
17    end
18    PatchQ_RM  $p, e$ 
19  end
20 end
21 return Distance( $S, G$ ) - Distance( $S', G'$ )

```

Interior defect removal. The first if branch handles interior defect removal. As shown in Section IV, the optimal removal of defective interior qubits can be achieved simply by applying either DataQ_RM or PatchQ_RM, depending on the qubit type. This simple strategy also achieves optimal removal even for complex defect patterns, since DataQ_RM and PatchQ_RM commute. This commutativity ensures that the removal of neighboring qubits does not interfere with each other, preserving the optimality of the strategy.

Comparison with ASC. ASC solely employs the DataQ_RM instruction even for defective syndrome qubits. For removing a defective syndrome qubit, ASC must apply DataQ_RM four times to remove adjacent data qubits, even if they are not defective. This can result in an unnecessary loss of code distance. For example, the deformed code produced by ASC in Fig. 7(a) has a Z-distance of only 3, while our strategy can preserve it to be 5.

Boundary defect removal. The removal of boundary defective qubits is achieved through PatchQ_RM (Fig. 6(c)). However, unlike the interior case where a larger stabilizer can be formed to provide additional error detection capabilities (Fig. 6(a)(b)),

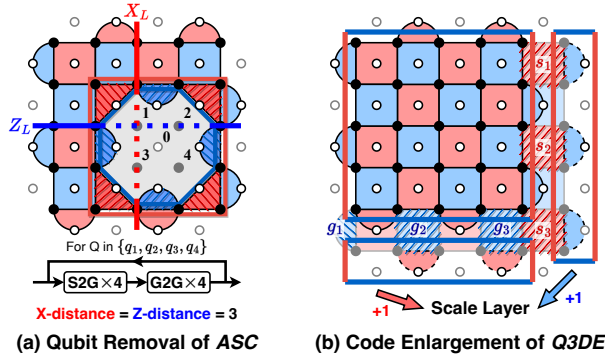


Fig. 7. Illustration of ASC and Q3DE. (a) The resulting code of ASC has X - and Z -distance both equal to 3, while our instruction Fig. 6(b) leads to a code with Z -distance 5 and X -distance 3. (b) Code enlargement of Q3DE equates to multiple `PatchQ_ADD` instructions.

simply applying `PatchQ_RM` leads to suboptimal code distance. Thus, we have to strategically apply `G2S` to introduce new stabilizers for extra protection. Especially in the corner case, we have to carefully choose from which edge to choose the gauge operator for conversion, to balance the distances X and Z . For example, for the defective data qubit q_0 in the top right corner of Fig. 8, we can convert either Z_q or X_q to a stabilizer. In the *balancing* function, we select the one that balances the X - and Z -code distances, reflected by the length of the boundaries (red and blue lines) to ensure that the deformed code remains resilient to both X - and Z -errors.

Comparison with ASC. ASC disables defective qubits on the boundary, disregarding their impact on the X -, Z -distances. As Fig. 8 shows, ASC converts the gauge operator Z_0 into stabilizer to minimize the number of disabled qubits, leading to a smaller Z -code distance than FlexiSCD.

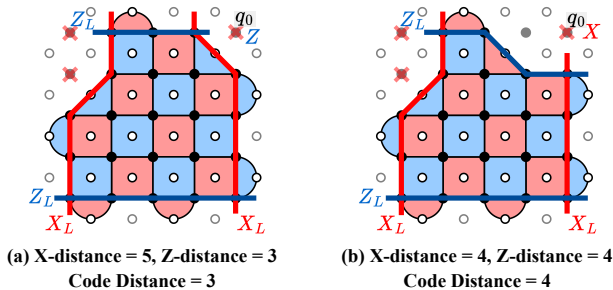


Fig. 8. Convert the right gauge operator into stabilizer to balance the X -, Z -distance. (a) ASC converts the gauge operator Z_0 into stabilizer, leading to unbalanced X -, Z -distance and a smaller code distance. (b) FlexiSCD converts the gauge operator X_0 into stabilizer, leading to balanced X -, Z -distance and a larger code distance.

B. Adaptive Enlargement Subroutine

This subroutine receives the deformed code of the *Defect Removal Subroutine* and efficiently restores the lost code distance by introducing new qubits. As illustrated in Algorithm 2, this enlargement process addresses defects in the newly introduced qubits and ensure a restoration to the original code distance.

Code enlargement with defective patches. After defect removal, we evaluate the reduction in both X - and Z -code

Algorithm 2: Adaptive Enlargement Subroutine

Input: stabilizer set S , gauge set G , defective qubit set D , original code distance $Dist$, current code distance $dist_X, dist_Z$

Output: stabilizer set S' , gauge set G'

```

1 Defects = ∅
2 while  $dist_X < Dist$  or  $dist_Z < Dist$  do
3   if  $dist_X < Dist$  then
4      $layer_1 = \text{find\_layer}(X_{L1})$ 
5     for  $patch \in layer_1$  do
6       if Exist  $d_i \in patch \cap D$  then
7         Find  $X$ -type  $patch_2$  that  $d_i \in patch_2$ 
8          $layer_1 = layer_1 \cup patch_2$ 
9          $D = D - d_i$ 
10         $Defects = Defects + d_i$ 
11      end
12    end
13     $layer_2 = \text{find\_layer}(X_{L2})$ 
14    ... similar to  $layer_1$ 
15     $layer, X_L = \min(layer_1, layer_2)$ 
16    for  $patch \in layer$  do
17      | PatchQ_ADD  $patch, X_L$ 
18    end
19     $dist_X = dist_X + 1$ 
20  else
21    | ... similar to  $dist_Z$ 
22  end
23  for  $d_i \in Defects$  do
24    | Apply Algorithm 1 to remove  $d_i$ 
25  end
26 end

```

distances compared to the ideal surface code. Calculating the code distance for every patch added to the surface code could be inefficient. In the `find_layer` function, we first identify a set of patches that can increase the code distance by at least one unit of the relevant type, assuming that the identified layer is defect-free.

However, new layers may contain defects, which invalidates our assumption. For example, in Fig. 10 (a), defective qubits q_1 and q_2 are removed, resulting in an irregular boundary that hinders regular enlargement. Similarly, in Fig. 10 (c), the defective qubit q_0 in the prospective scale layer also complicates the enlargement.

To solve this problem, FlexiSCD combines the instruction `PatchQ_ADD` with the qubit removal subroutine `DataQ_RM`, `SyndromeQ_RM`, `PatchQ_RM`, as shown in line 24 in Algorithm 2. Initially, defective qubits are temporarily disregarded to facilitate the regular enlargement. Subsequently, these defective qubits are excluded using our qubit removal instructions, resulting in an enlarged code with defects removed as the output of the Code Deformation Unit (Fig. 10 (b) (d)). To execute the deformation process, qubits are introduced in the appropriate

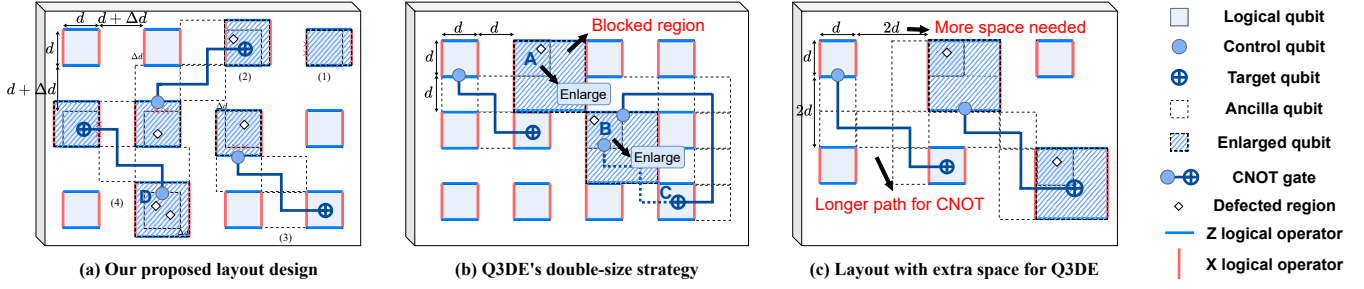


Fig. 9. (a) Our proposed layout with inter-placing width $d + \Delta d$ can facilitate long range logical operation with lower qubit overheads while preserving code distance d of the communication channel. (b) The layout for Q3DE's double-size strategy. (c) To effectively facilitate the qubit communication in Q3DE's method, an inter-space of $2d$ is necessary, introducing a significant qubit overhead.

state all at once, and stabilizers in the new code are measured. Importantly, this seamless integration of qubit removal and enlargement is facilitated by the unified gauge transformation perspective underlying these deformation instructions.

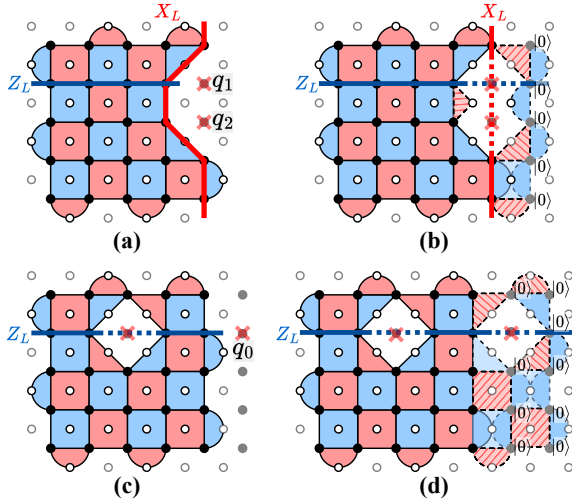


Fig. 10. Enlargement while addressing defects. (a) Removed defects create an irregular boundary. (b) Enlarging on the irregular boundary in (a). (c) Defect can occur on prospective enlarging layers. (d) Enlarging by a qubit layer with a defect in (c).

VI. THE LAYOUT GENERATOR

FlexiSCD's layout generator aims to facilitate communication between surface codes in the presence of potential code enlargement due to defect mitigation. The key idea is to introduce an additional Δd inter-space, as shown in Fig. 9(a), to accommodate enlargements of up to size Δd (or even $2\Delta d$ if enlarging in both directions). The parameter Δd is determined by the defect error model, chosen such that enlarging within size Δd can effectively restore the code distance of the deformed code with high probability. Therefore, the communication channel of width d will only be compromised by code enlargement with a negligible probability.

Comparison with Q3DE. As illustrated in Fig. 7 (b), Q3DE supports fixed enlargement only, whereas our FlexiSCD allows the introduction of only the necessary number of patches to restore the code distance, resulting in savings in qubit

resources needed for incorporation into the code. Moreover, the basic process in Q3DE lacks the capability to address irregular boundaries caused by defects or defects occurring on newly introduced qubits. Consequently, Q3DE may inadvertently introduce additional defective qubits during the enlargement process, leading to an increase in error sources that counteract the intended function of the introduced redundant qubits. This failure to effectively mitigate defects can result in a logical error rate that exceeds expectations.

FlexiSCD's layout generator. The output layout is determined by three parameters:

(1) *Logical qubit number N .* The logical qubits in the layout should be the algorithmic qubits needed for the quantum program, plus the additional qubits essential for facilitating quantum computation, such as logical qubits prepared in magic states for implementing logical T gates [41]. These logical qubits are arranged in a lattice on a plane, with each one encoded within a surface code and equally spaced apart from one another.

(2) *Code distance d .* The code distance d should be chosen sufficiently large to maintain a sufficiently low logical error rate, ensuring that the failure rate α_{fail} of the program execution remains below a certain threshold, such as 0.1%. The failure rate can be estimated based on the logical error rate and features of the quantum program, such as the number of logical gates and the space-time cost of logical gates. For further details on this estimation, please refer to [42], [50].

(3) *Additional inter-space Δd .* We present an error model for defects that allows us to estimate the probability of the communication channel being blocked. We assume that defects occurring on each physical qubit follow a Poisson process with rate ρ , lasting for a time T , and with a maximal size of D . Thus, the number of defects on a patch follows a Poisson distribution with parameter $\lambda = 2d^2\rho T$, since a surface code of code distance d contains roughly $2d^2$ physical qubits. Therefore, the probability of having k defects on a code is $p(k) = \frac{\lambda^k}{k!} e^{-\lambda}$. The additional inter-space Δd can accommodate the enlargement for mitigating $\lfloor \Delta d/D \rfloor$ defects without compromising the communication channel. The probability of this protection failing and the channel becoming blocked is:

$$p_{block} = 1 - \sum_{k=0}^{\lfloor \Delta d/D \rfloor} p(k) \quad (1)$$

TABLE II
RESULTS OF Q3DE, ASC AND FLEXISCD FOR VARIOUS PROGRAMS WITH DIFFERENT SCALE

Benchmark					Q3DE		ASC		FlexiSCD	
Name	# CX	# T	# qubit	d	# physical qubit	Retry risk	# physical qubit	Retry risk	# physical qubit	Retry risk
Simon -400-1000	3.02×10^5	0	400	19	1.46×10^6	OverRuntime	1.46×10^6	53.1%	1.80×10^6	1.51%
				21	1.79×10^6	OverRuntime	1.79×10^6	7.28%	2.15×10^6	0.17%
Simon -900-1500	1.01×10^6	0	900	21	3.73×10^6	OverRuntime	3.73×10^6	46.7%	4.49×10^6	1.09%
				23	4.47×10^6	OverRuntime	4.47×10^6	6.14%	5.30×10^6	0.12%
RCA -225-500	8.96×10^5	7.84×10^5	225	21	1.08×10^6	OverRuntime	1.08×10^6	41.9%	1.30×10^6	0.98%
				23	1.30×10^6	OverRuntime	1.30×10^6	5.63%	1.54×10^6	0.11%
RCA -729-100	5.82×10^5	5.10×10^5	729	21	3.07×10^6	OverRuntime	3.07×10^6	76.6%	3.70×10^6	1.79%
				23	3.69×10^6	OverRuntime	3.69×10^6	10.2%	4.37×10^6	0.20%
QFT -25-160	1.02×10^5	1.87×10^8	25	23	2.39×10^5	OverRuntime	2.39×10^5	61.4%	2.85×10^5	1.20%
				25	2.82×10^5	OverRuntime	2.82×10^5	7.83%	3.32×10^5	0.13%
QFT -100-20	2.30×10^5	1.58×10^9	100	25	0.78×10^6	OverRuntime	0.78×10^6	$\sim 100\%$	0.92×10^6	1.69%
				27	0.91×10^6	OverRuntime	0.91×10^6	12.6%	1.06×10^6	0.18%
Grover -9-80	1.36×10^5	1.99×10^8	9	23	1.29×10^5	OverRuntime	1.29×10^5	57.3%	1.54×10^5	1.12%
				25	1.51×10^5	OverRuntime	1.51×10^5	7.23%	1.79×10^5	0.12%
Grover -16-2	4.29×10^5	1.13×10^9	16	25	2.12×10^5	OverRuntime	2.12×10^5	56.0%	2.50×10^5	0.93%
				27	2.47×10^5	OverRuntime	2.47×10^5	7.01%	2.88×10^5	0.10%

A desired Δd should be chosen as the smallest value such that the block probability is below a certain threshold α_{block} , such as $\alpha_{block} = 0.01$.

For example, in experiment [22], cosmic-rays attack a 26-qubit superconducting device roughly every 10s, with each attack lasting for 25ms, and the number of affected qubits up to 24. In this case, $\rho = 0.1\text{Hz}/26$, $T = 25\text{ms}$, and $D \approx 4$. For a typical surface code of size $d = 27$ [50], its Poisson parameter is $\lambda = 0.14$. Here, we can choose $\Delta d = 4$ because $p_{block} = 1 - p(0) - p(1) \approx 0.0089 < 0.01 = \alpha_{block}$.

Comparison with Q3DE layout. Q3DE’s layout poses challenges on logical qubit communication due to its double-size enlargement scheme, which entirely obstructs the space between codes used for executing logical operations Fig. 9(b). It has the following major limitations:

(1) *Space-time overhead of logical operations.* The blocked channel may lead to space overhead for long-distance logical operations. For example, in Fig. 9(b), the CNOT gate from qubit B to C must traverse a longer path (solid line) instead of the shorter one (dotted lines) due to the enlarged qubit B . Moreover, the blocked channel can result in severe time overhead. Logical operations may become unfeasible due to blocked paths, such as the CNOT gate from qubit A to B . In such cases, the program must be paused for a long time (thousands of QEC cycles) until the effects of defects subside, and the code shrinks back to its original size, making the ancilla path available again. In contrast, our layout with an extra inter-space Δd effectively suppresses the block probability, thus reducing the space-time cost of logical operations to a nearly optimal level.

(2) *Qubit resource for facilitating communication.* It’s possible for the size-doubling strategy in Q3DE to achieve nearly optimal space and time costs, but it requires a $2d$ inter-space (Fig. 9(c)) to accommodate both code enlargement and ancilla paths of distance d . However, this results in a significant qubit resource overhead of $(\frac{3d}{2d})^2 = 2.25$ times. In contrast, our layout introduces a lower overhead since Δd must be smaller

than d . This overhead remains mild, especially when Δd is relatively small compared to the code distance d .

VII. IMPLEMENTATION AND EVALUATION

A. Experimental Setup

Evaluation setting. We use the Stim stabilizer circuit simulator [51] and the PyMatching [52] decoder for our numerical simulations. For program compilation, we employ the lattice surgery framework described in [42], [53], along with the T factory for implementing logical T gates using magic state distillation strategies [40].

Benchmark programs. We have selected several quantum programs designed to tackle real-world challenges. These programs include Simon’s algorithm [54], Ripple Carry Adder (RCA) [55], Quantum Fourier Transform (QFT) [56], and Grover’s algorithm [5]. The first suffix of the name indicates the number of logical qubits used, while the second suffix represents the number of repetitions. For instance, “QFT-100-20” indicates the task of 20 QFT layers on 100 qubits, a common scenario used in more complex algorithms like Shor’s algorithm [4].

Metric. For evaluation, we consider three key metrics. First, the *physical qubit count* encompasses all data and ancilla qubits used in the quantum program’s layout. It quantifies the qubit resources required for the task, with lower values being preferred. Second, the *retry risk*, as defined by [50], represents the probability of an uncorrectable logical error occurring in the program, which will lead to an incorrect task result that necessitates retry. This metric indicates the error rate of task results, with lower values being preferred. Third, the *throughput* of non-local operations represents the average number of operations executed in one cycle, with higher values being preferred. This metric indicates the layout’s ability to execute non-local operations (CNOT and T gates) in parallel, which can significantly impact task runtime, particularly when compared to local operations.

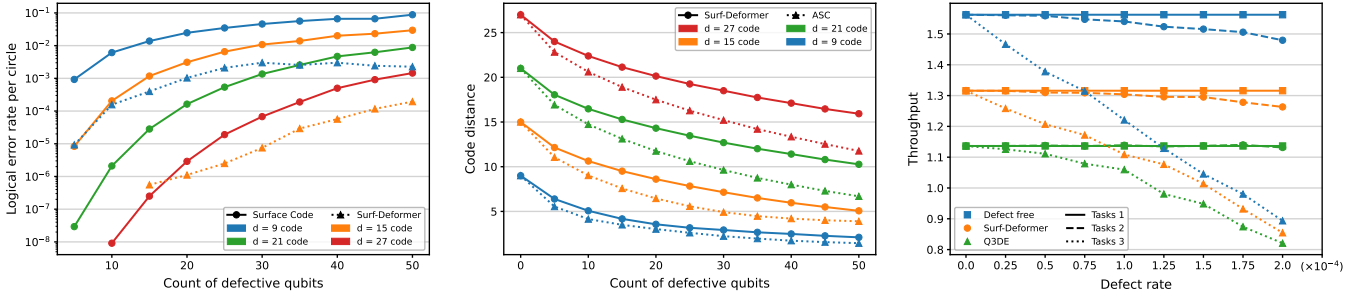


Fig. 11. (a) Logical error rate of with qubit removal by FlexiSCD and without any treatment. (b) Cost in distance recovery. (c) Throughput vs Defect.

Error model. We adopt an error model similar to [2]. The physical error rate of each qubit is assumed to be $p = 10^{-3}$. For dynamic defects, each physical qubit experiences a dynamic defect event following an exponential distribution with an average event rate of $\lambda = 1/(26 \times 10 \text{ s})$ [22]. When a physical qubit is attacked, the adjacent 24 qubits are affected, resulting in a defective region of size 4. The physical error rate of qubits in the affected region increases to approximately 50% and lasts for $T = 25 \text{ ms}$, equivalent to approximately 25000 QEC cycles.

B. Overall Performance

We compare our FlexiSCD with two previous frameworks, Q3DE method [2] and adaptive surface code (ASC) [1], on benchmark programs mentioned in Section VII-A. The results are presented in Table II. We evaluate these tasks on surface codes of appropriate distances chosen to meet the target retry risk levels of 1% and 0.1% in our framework. Overall, our FlexiSCD in Table II demonstrates a consistently better performance. In particular, we highlight the following three observations:

- 1) All tasks processed by Q3DE exhibit a retry risk of $\sim 100\%$, indicating an inability to mitigate the impact of dynamic defects. This limitation stems from its enlargement operation with a fixed layout, which causes the ancilla space near the defective qubits to become blocked. Additionally, the large scale of tasks necessitates high-fidelity logical qubits, implying a large code distance d for the surface code. With more qubits used to encode a logical qubit, there is a higher probability of the qubit blocks being attacked by defect events. Consequently, most qubit blocks become enlarged in Q3DE, and a significant portion of the ancilla paths are blocked. Fewer or even no available ancilla paths for executing non-local operations result in the high retry risk.
- 2) Without the ability to recover the decreased distance caused by removing defective qubits, the retry risk of tasks executed by ASC is 35x-70x higher than those by our FlexiSCD. This disparity arises from the task's retry risk being determined by the worst qubit blocks during runtime, since a single logical error on any logical qubit can lead to the failure of the entire task. Failure to restore a low-distance logical qubit to the original

required distance d for the task significantly amplifies the retry risk.

- 3) With FlexiSCD's layout, it requires only around 20% more physical qubits to resolve the communication blocking issue and achieve a low retry risk. Moreover, even with the same number of physical qubits, FlexiSCD still outperforms ASC. For example, in the task "QFT-100-20," FlexiSCD with $d = 25$ and $\Delta d = 4$ and ASC with $d = 27$ both use roughly 9×10^5 physical qubits. However, the retry risk of FlexiSCD is still 6.3x lower than that of ASC.

C. Analysis on Sub-components

In this section, we demonstrate the superior performance of our FlexiSCD due to its adaptive deformation framework and layout. Our approach excels in saving qubit resources, maintaining the QEC capability of the deformed code, and enhancing surface code communication compared to other methods. We have conducted a series of experiments to showcase these advantages.

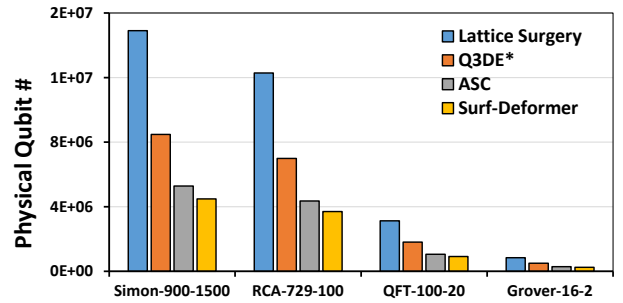


Fig. 12. Physical qubit counts required to achieve a retry risk of approximately 1%. Q3DE* stands for the revised illustrated in Fig. 9(c).

Qubit resource saving. We demonstrate the substantial resource savings achieved by FlexiSCD by comparing the physical qubit count required for the layout to achieve a 1% retry risk with different methods. Our comparison includes Lattice Surgery, the revised version of Q3DE, and ASC. In the revised Q3DE, we adjust the inter-space to $2d$ to prevent the enlargement from blocking surrounding communication paths, as illustrated in Fig. 9(c). As depicted in Fig. 12, FlexiSCD requires significantly fewer qubits compared to all previous methods, approximately 75% less than Lattice Surgery, 50% less than Q3DE, and 15% less than ASC.

Improved logical error rate by qubit removal. In Fig. 11(a), we compare the logical error rates of surface codes with and without defective qubits removed by FlexiSCD, across different numbers of defective qubits. We do not present the cases for $d = 21$ and $d = 27$ because the logical error rates are so low that numerical simulations cannot provide reasonable estimations.

The results show that FlexiSCD significantly enhances the logical error rate by removing defects. Codes with defects removed achieve comparable logical error rates to those without any treatment, despite having much smaller code distances. For instance, when there are 10 defective qubits, a distance-9 code with defects removed shows a similar logical error rate to a distance-15 code without any treatment. This also underscores that simply expanding the code size while retaining defective qubits, as in Q3DE, cannot effectively improve logical error rates as expected.

Enhanced code distance by adaptive defect removal. We compare the cost of distance recovery of FlexiSCD and previous methods such as ASC that use oversimplified deformation operations. Fig. 11(b) gives the code distance of defective codes of different original sizes, w.r.t. varying number of defective qubits. It indicates that our method can preserve the code distance better than the previous methods, leading to a lower cost when recovering the code distance through enlargement. Additionally, the advantage of our method becomes more significant on codes of larger size and when there are more defective qubits.

Parallelism improvement by FlexiSCD’s layout. In Fig. 11(c), we compare the efficiency of qubit communication using the layouts in three schemes: (1) FlexiSCD, (2) Q3DE with d inter-space, and (3) classical lattice surgery (LS), representing optimal runtime. We consider 100 logical qubits and three sets of tasks, each comprising 5 tasks with 25 CNOT gates on 50 distinct logical qubits. The tasks in each set can be completed in 16, 19, and 22 time-steps on the LS layout, respectively, indicating three levels of parallelism. We then sample defects 100 times for each task and compute the average throughput of each task set using the layouts in FlexiSCD and Q3DE.

The results indicate that as the defect rate increases, the throughput significantly drops for the Q3DE layout, whereas it only experiences a slight decline with our layout. This is because expanding all the defective code to a $2d$ size severely blocks the ancilla paths for long-range CNOT gates, resulting in a much longer execution time, while the additional Δd space in our layout significantly reducing the probability of ancilla paths being blocked. Therefore, the FlexiSCD layout effectively facilitates the computation among logical qubits.

VIII. RELATED WORK

In this section, we present a broader perspective on approaches for addressing dynamic defects in quantum hardware. Generally, there are three main directions to consider:

(1) Hardware-level solutions. Dynamic defects can be mitigated at the hardware level to reduce their incidence rate. Physical techniques such as shielding [24], [30], phonon

downconversion [57], [58], and metallic covers [59] can help mitigate the burst of quasiparticles induced by radiation materials and cosmic rays, which is a main source of qubit decoherence. Various mitigation methods on chips [21], [60] are also proposed. However, these hardware-level solutions alone are often insufficient to reduce the logical error rate to a level where meaningful quantum computations, which can take several hours [50], can be effectively executed. Although preventing these defects at the hardware level is challenging, specialized hardware detectors [31], [32] can often locate them accurately at runtime with statistical methods.

(2) Software-level solution. To address dynamic defects that involve varying error rates, methods like [2], [61], [62], [63] estimate modified error rates based on historical syndrome data and then adjust the error rates in the decoders such as MWPM [47], [64], [65], [66], [67], [68]. Various error mitigation approaches [69], [70], [71] based on statistical methods are also proposed. However, these methods becomes ineffective when the physical error rate is considerably high or the errors can possible propagate, but these are often the case with dynamic defects, where defected qubits can have error rates near 50% and affect the integrity of adjacent qubits [22], [25].

(3) QEC-level solution. Theoretical frameworks have been established for converting one stabilizer code to another [48], [72], [73], [74], [75], [76] by modifying the code through a series of measurements. However, these methods either potentially modify the encoded information [48], [75], or ignore the hardware constraints on qubit connectivity [76], limiting their code conversion procedure for practical use. On the other hand, approaches such as [1], [2], [77] design new codes based on the structure of the underlying hardware. However, these methods are inefficient in utilizing the remaining intact qubits, do not detail the specific deformation procedure, and overlook the feasibility of communication between logical qubits.

IX. CONCLUSION

In this work, we introduce a novel deformation framework FlexiSCD, which expands the existing surface code instruction set by integrating adaptive defect mitigation functionalities. Based on four meticulously designed deformation instructions, FlexiSCD creates a larger design space than previous work, enabling optimized deformation processes tailored to specific defects. When combined with a new adaptive code layout, FlexiSCD significantly enhances qubit communication efficiency and reduces logical error rates with only mild additional qubit resource. Comprehensive evaluations show that FlexiSCD produces deformed codes with better QEC capabilities and more efficient qubit communication. FlexiSCD serves as a versatile tool for effectively addressing defects in surface codes across various quantum platforms.

REFERENCES

- [1] Adam Siegel, Armands Strikis, Thomas Flatters, and Simon Benjamin. Adaptive surface code for quantum error correction in the presence of temporary or permanent defects. *Quantum*, 7:1065, 2023.

- [2] Yasunari Suzuki, Takanori Sugiyama, Tomochika Arai, Wang Liao, Koji Inoue, and Teruo Tanimoto. Q3de: A fault-tolerant quantum computer architecture for multi-bit burst errors by cosmic rays. In *2022 55th IEEE/ACM International Symposium on Microarchitecture (MICRO)*, pages 1110–1125. IEEE, 2022.
- [3] John Preskill. Quantum computing in the nisq era and beyond. *Quantum*, 2:79, 2018.
- [4] Peter W Shor. Polynomial-time algorithms for prime factorization and discrete logarithms on a quantum computer. *SIAM review*, 41(2):303–332, 1999.
- [5] Lov K Grover. A fast quantum mechanical algorithm for database search. In *Proceedings of the twenty-eighth annual ACM symposium on Theory of computing*, pages 212–219, 1996.
- [6] Alberto Peruzzo, Jarrod McClean, Peter Shadbolt, Man-Hong Yung, Xiao-Qi Zhou, Peter J Love, Alán Aspuru-Guzik, and Jeremy L O’Brien. A variational eigenvalue solver on a photonic quantum processor. *Nature communications*, 5(1):4213, 2014.
- [7] Peter W Shor. Fault-tolerant quantum computation. In *Proceedings of 37th conference on foundations of computer science*, pages 56–65. IEEE, 1996.
- [8] A Robert Calderbank and Peter W Shor. Good quantum error-correcting codes exist. *Physical Review A*, 54(2):1098, 1996.
- [9] Andrew Steane. Multiple-particle interference and quantum error correction. *Proceedings of the Royal Society of London. Series A: Mathematical, Physical and Engineering Sciences*, 452(1954):2551–2577, 1996.
- [10] Sergey B Bravyi and A Yu Kitaev. Quantum codes on a lattice with boundary. *arXiv preprint quant-ph/9811052*, 1998.
- [11] Héctor Bombín and Miguel A Martin-Delgado. Optimal resources for topological two-dimensional stabilizer codes: Comparative study. *Physical Review A*, 76(1):012305, 2007.
- [12] Hector Bombin and Miguel Angel Martin-Delgado. Topological quantum distillation. *Physical review letters*, 97(18):180501, 2006.
- [13] Peter W Shor. Scheme for reducing decoherence in quantum computer memory. *Physical review A*, 52(4):R2493, 1995.
- [14] A Yu Kitaev. Fault-tolerant quantum computation by anyons. *Annals of physics*, 303(1):2–30, 2003.
- [15] Austin G Fowler, Matteo Mariantoni, John M Martinis, and Andrew N Cleland. Surface codes: Towards practical large-scale quantum computation. *Physical Review A*, 86(3):032324, 2012.
- [16] Simon J Devitt, William J Munro, and Kae Nemoto. Quantum error correction for beginners. *Reports on Progress in Physics*, 76(7):076001, 2013.
- [17] Suppressing quantum errors by scaling a surface code logical qubit. *Nature*, 614(7949):676–681, 2023.
- [18] Youwei Zhao, Yangsen Ye, He-Liang Huang, Yiming Zhang, Dachao Wu, Huijie Guan, Qingling Zhu, Zuolin Wei, Tan He, Sirui Cao, et al. Realization of an error-correcting surface code with superconducting qubits. *Physical Review Letters*, 129(3):030501, 2022.
- [19] Dolev Bluvstein, Simon J Evered, Alexandra A Geim, Sophie H Li, Hengyun Zhou, Tom Manovitz, Sepehr Ebadi, Madelyn Cain, Marcin Kalinowski, Dominik Hangleiter, et al. Logical quantum processor based on reconfigurable atom arrays. *Nature*, 626(7997):58–65, 2024.
- [20] Sebastian Krinner, Nathan Lacroix, Ants Remm, Agustin Di Paolo, Elie Genois, Catherine Leroux, Christoph Hellings, Stefania Lazar, Francois Swiadek, Johannes Herrmann, et al. Realizing repeated quantum error correction in a distance-three surface code. *Nature*, 605(7911):669–674, 2022.
- [21] John M Martinis. Saving superconducting quantum processors from decay and correlated errors generated by gamma and cosmic rays. *npj Quantum Information*, 7(1):90, 2021.
- [22] Matt McEwen, Lara Faoro, Kunal Arya, Andrew Dunsworth, Trent Huang, Seon Kim, Brian Burkett, Austin Fowler, Frank Arute, Joseph C Bardin, et al. Resolving catastrophic error bursts from cosmic rays in large arrays of superconducting qubits. *Nature Physics*, 18(1):107–111, 2022.
- [23] Christopher D Wilen, S Abdullah, NA Kurinsky, C Stanford, L Cardani, G d’Imperio, C Tomei, L Faoro, LB Ioffe, CH Liu, et al. Correlated charge noise and relaxation errors in superconducting qubits. *Nature*, 594(7863):369–373, 2021.
- [24] Antti P Vepsäläinen, Amir H Karamlou, John L Orrell, Akshunna S Dogra, Ben Loer, Francisca Vasconcelos, David K Kim, Alexander J Melville, Bethany M Niedzielski, Jonilyn L Yoder, et al. Impact of ionizing radiation on superconducting qubit coherence. *Nature*, 584(7822):551–556, 2020.
- [25] Natalie C Brown, Michael Newman, and Kenneth R Brown. Handling leakage with subsystem codes. *New Journal of Physics*, 21(7):073055, 2019.
- [26] Iris Cong, Harry Levine, Alexander Keesling, Dolev Bluvstein, Sheng-Tao Wang, and Mikhail D. Lukin. Hardware-efficient, fault-tolerant quantum computation with rydberg atoms, 2022.
- [27] E Gümüş, Danial Majidi, Danilo Nikolić, Patrick Raif, Bayan Karimi, Joonas T Peltonen, Elke Scheer, Jukka P Pekola, Hervé Courtois, Wolfgang Belzig, et al. Calorimetry of a phase slip in a josephson junction. *Nature Physics*, 19(2):196–200, 2023.
- [28] Matthew L Day, Pei Jiang Low, Brendan White, Rajibul Islam, and Crystal Senko. Limits on atomic qubit control from laser noise. *npj Quantum Information*, 8(1):72, 2022.
- [29] JJ Burnett, A Bengtsson, M Scigliuzzo, D Niepce, M Kudra, P Delsing, and J Bylander. Decoherence benchmarking of superconducting qubits. *npj quantum inf.* 5. 2019.
- [30] Laura Cardani, Francesco Valenti, Nicola Casali, Gianluigi Catelani, Thibault Charpentier, Massimiliano Clemenza, Ivan Colantoni, Angelo Cruciani, G D’Imperio, Luca Gironi, et al. Reducing the impact of radioactivity on quantum circuits in a deep-underground facility. *Nature communications*, 12(1):2733, 2021.
- [31] James T Farmer, Azarin Zarassi, Darian M Hartsell, Evangelos Vlachos, Haimeng Zhang, and Eli M Levenson-Falk. Continuous real-time detection of quasiparticle trapping in aluminum nanobridge josephson junctions. *Applied Physics Letters*, 119(12), 2021.
- [32] Willemijn Uilhoorn, James G Kroll, Arno Bargerbos, Syed D Nabi, Chung-Kai Yang, Peter Krogstrup, Leo P Kouwenhoven, Angela Kou, and Gijs de Lange. Quasiparticle trapping by orbital effect in a hybrid superconducting-semiconducting circuit. *arXiv preprint arXiv:2105.11038*, 2021.
- [33] Kaitlin N Smith, Gokul Subramanian Ravi, Jonathan M Baker, and Frederic T Chong. Scaling superconducting quantum computers with chiplet architectures. In *2022 55th IEEE/ACM International Symposium on Microarchitecture (MICRO)*, pages 1092–1109. IEEE, 2022.
- [34] Thomas M Stace, Sean D Barrett, and Andrew C Doherty. Thresholds for topological codes in the presence of loss. *Physical review letters*, 102(20):200501, 2009.
- [35] Thomas M Stace and Sean D Barrett. Error correction and degeneracy in surface codes suffering loss. *Physical Review A*, 81(2):022317, 2010.
- [36] James M Auger, Hussain Anwar, Mercedes Gimeno-Segovia, Thomas M Stace, and Dan E Browne. Fault-tolerance thresholds for the surface code with fabrication errors. *Physical Review A*, 96(4):042316, 2017.
- [37] Shota Nagayama, Austin G Fowler, Dominic Horsman, Simon J Devitt, and Rodney Van Meter. Surface code error correction on a defective lattice. *New Journal of Physics*, 19(2):023050, 2017.
- [38] Sophia Fuhui Lin, Joshua Vizlai, Kaitlin N Smith, Gokul Subramanian Ravi, Charles Yuan, Frederic T Chong, and Benjamin J Brown. Codesign of quantum error-correcting codes and modular chiplets in the presence of defects. In *Proceedings of the 29th ACM International Conference on Architectural Support for Programming Languages and Operating Systems, Volume 2*, pages 216–231, 2024.
- [39] Dominic Horsman, Austin G Fowler, Simon Devitt, and Rodney Van Meter. Surface code quantum computing by lattice surgery. *New Journal of Physics*, 14(12):123011, 2012.
- [40] Austin G Fowler and Craig Gidney. Low overhead quantum computation using lattice surgery. *arXiv preprint arXiv:1808.06709*, 2018.
- [41] Michael Beverland, Vadym Kliuchnikov, and Eddie Schoute. Surface code compilation via edge-disjoint paths. *PRX Quantum*, 3(2):020342, 2022.
- [42] Daniel Litinski. A game of surface codes: Large-scale quantum computing with lattice surgery. *Quantum*, 3:128, 2019.
- [43] Tyler LeBlond, Ryan S Bennink, Justin G Lietz, and Christopher M Seck. Tiscc: A surface code compiler and resource estimator for trapped-ion processors. In *Proceedings of the SC’23 Workshops of The International Conference on High Performance Computing, Network, Storage, and Analysis*, pages 1426–1435, 2023.
- [44] Michael A Nielsen and Isaac L Chuang. *Quantum computation and quantum information*. Cambridge university press, 2010.
- [45] Daniel Gottesman. Class of quantum error-correcting codes saturating the quantum hamming bound. *Physical Review A*, 54(3):1862, 1996.
- [46] Daniel Gottesman. The heisenberg representation of quantum computers, 1998.

- [47] Eric Dennis, Alexei Kitaev, Andrew Landahl, and John Preskill. Topological quantum memory. *Journal of Mathematical Physics*, 43(9):4452–4505, 2002.
- [48] Christophe Vuillot, Lingling Lao, Ben Criger, Carmen García Almudéver, Koen Bertels, and Barbara M Terhal. Code deformation and lattice surgery are gauge fixing. *New Journal of Physics*, 21(3):033028, 2019.
- [49] David Poulin. Stabilizer formalism for operator quantum error correction. *Physical review letters*, 95(23):230504, 2005.
- [50] Craig Gidney and Martin Ekerå. How to factor 2048 bit rsa integers in 8 hours using 20 million noisy qubits. *Quantum*, 5:433, 2021.
- [51] Craig Gidney. Stim: a fast stabilizer circuit simulator. *Quantum*, 5:497, 2021.
- [52] Oscar Higgott. Pymatching: A python package for decoding quantum codes with minimum-weight perfect matching. *ACM Transactions on Quantum Computing*, 3(3):1–16, 2022.
- [53] George Watkins, Hoang Minh Nguyen, Varun Seshadri, Keelan Watkins, Steven Pearce, Hoi-Kwan Lau, and Alexandru Paler. A high performance compiler for very large scale surface code computations. *arXiv preprint arXiv:2302.02459*, 2023.
- [54] Daniel R Simon. On the power of quantum computation. *SIAM journal on computing*, 26(5):1474–1483, 1997.
- [55] Yasuhiro Takahashi and Noboru Kunihiro. A linear-size quantum circuit for addition with no ancillary qubits. *Quantum Information & Computation*, 5(6):440–448, 2005.
- [56] Don Coppersmith. An approximate fourier transform useful in quantum factoring. *arXiv preprint quant-ph/0201067*, 2002.
- [57] K Karatsu, A Endo, J Bueno, PJ De Visser, R Barends, DJ Thoen, V Murugesan, N Tomita, and JJA Baselmans. Mitigation of cosmic ray effect on microwave kinetic inductance detector arrays. *Applied Physics Letters*, 114(3), 2019.
- [58] V Iqbal, J Ku, A Ballard, CP Larson, E Yelton, CH Liu, S Patel, R McDermott, and BLT Plourde. Phonon downconversion to suppress correlated errors in superconducting qubits. *Nature Communications*, 13(1):6425, 2022.
- [59] Xianchuan Pan, Yuxuan Zhou, Haolan Yuan, Lifu Nie, Weiwei Wei, Libo Zhang, Jian Li, Song Liu, Zhi Hao Jiang, Gianluigi Catelani, et al. Engineering superconducting qubits to reduce quasiparticles and charge noise. *Nature Communications*, 13(1):7196, 2022.
- [60] Matt McEwen, Dvir Kafri, Z Chen, Juan Atalaya, KJ Satzinger, Chris Quintana, Paul Victor Klimov, Daniel Sank, C Gidney, AG Fowler, et al. Removing leakage-induced correlated errors in superconducting quantum error correction. *Nature communications*, 12(1):1761, 2021.
- [61] Josu Etxezarreta Martinez, Patricio Fuentes, Pedro Crespo, and Javier Sergey Bravyi, Sarah Sheldon, Abhinav Kandala, David C Mckay, and Jay M Gambetta. Mitigating measurement errors in multiqubit experiments. *Physical Review A*, 103(4):042605, 2021.
- Garcia-Frias. Time-varying quantum channel models for superconducting qubits. *npj Quantum Information*, 7(1):115, 2021.
- [62] Oscar Higgott, Thomas C Bohdanowicz, Aleksander Kubica, Steven T Flammia, and Earl T Campbell. Improved decoding of circuit noise and fragile boundaries of tailored surface codes. *Physical Review X*, 13(3):031007, 2023.
- [63] Austin G Fowler, D Sank, J Kelly, R Barends, and John M Martinis. Scalable extraction of error models from the output of error detection circuits. *arXiv preprint arXiv:1405.1454*, 2014.
- [64] Austin G Fowler, Adam C Whiteside, and Lloyd CL Hollenberg. Towards practical classical processing for the surface code. *Physical review letters*, 108(18):180501, 2012.
- [65] Oscar Higgott and Craig Gidney. Sparse blossom: correcting a million errors per core second with minimum-weight matching, 2023.
- [66] Austin G Fowler. Optimal complexity correction of correlated errors in the surface code. *arXiv preprint arXiv:1310.0863*, 2013.
- [67] Nicolas Delfosse and Jean-Pierre Tillich. A decoding algorithm for css noise in quantum error correction via decoding graph re-weighting, 2023.
- [68] Hanrui Wang, Pengyu Liu, Yilian Liu, Jiaqi Gu, Jonathan Baker, Frederic T. Chong, and Song Han. Dgr: Tackling drifted and correlated noise in quantum error correction via decoding graph re-weighting, 2023.
- [69] Christophe Piveteau, David Sutter, Sergey Bravyi, Jay M Gambetta, and Kristan Temme. Error mitigation for universal gates on encoded qubits. *Physical review letters*, 127(20):200505, 2021.
- [70] Kristan Temme, Sergey Bravyi, and Jay M Gambetta. Error mitigation for short-depth quantum circuits. *Physical review letters*, 119(18):180509, 2017.
- [71] Ashley M Stephens, Zachary WE Evans, Simon J Devitt, and Lloyd CL Hollenberg. Asymmetric quantum error correction via code conversion. *Physical Review A*, 77(6):062335, 2008.
- [72] Charles D Hill, Austin G Fowler, David S Wang, and Lloyd CL Hollenberg. Fault-tolerant quantum error correction code conversion. *Quantum Information & Computation*, 13(5-6):439–451, 2013.
- [73] Yongsoo Hwang, Byung-Soo Choi, Young-chai Ko, and Jun Heo. Fault-tolerant conversion between stabilizer codes by clifford operations. *arXiv preprint arXiv:1511.02596*, 2015.
- [74] Héctor Bombín and Miguel Angel Martin-Delgado. Quantum measurements and gates by code deformation. *Journal of Physics A: Mathematical and Theoretical*, 42(9):095302, 2009.
- [75] Kristina R Colladay and Erich J Mueller. Rewiring stabilizer codes. *New Journal of Physics*, 20(8):083030, 2018.
- [76] Armands Strikis, Simon C Benjamin, and Benjamin J Brown. Quantum computing is scalable on a planar array of qubits with fabrication defects. *Physical Review Applied*, 19(6):064081, 2023.